

Multifunctional Triboelectric Nanogenerator-Enabled Structural Elements for Next Generation Civil Infrastructure Monitoring Systems

Qianyun Zhang, Kaveh Barri, Sadra R. Kari, Zhong Lin Wang, and Amir H. Alavi*

There is a critical shortage in research needed to explore a new class of multifunctional structural components that respond to their environment, empower themselves and self-monitor their condition. Here, the novel concept of triboelectric nanogenerator-enabled structural elements (TENG-SEs) is proposed to build the foundation for the next generation civil infrastructure systems with intrinsic sensing and energy harvesting functionalities. In order to validate the proposed concept, a proof-of-concept multifunctional composite rebars is developed with built-in TENG mechanisms. The developed prototypes function as structural reinforcements, nanogenerators, and distributed sensing mediums under external mechanical vibrations. Experiential and theoretical studies are performed to verify the electrical and mechanical performance of the developed self-powering and self-sensing composite structural components. The capability of the embedded structural elements to detect damage patterns in concrete beams at multiscale is demonstrated. Finally, it is discussed how this new class of TENG-SEs can revolutionize the large-scale distributed monitoring practices in civil infrastructure and construction fields.

1. Introduction

Since the early 1990s, catastrophic collapses of buildings and infrastructure have been frequently reported in the United States.^[1] Structural health monitoring (SHM) methods have been widely used to assess the performance of these structures and to identify damages at early stages.^[2] Smart sensor networks form the backbone of the SHM systems. They are typically used to measure physical quantities such as temperature, pressure, or strain. Strain is a key parameter to indicate the health condition of infrastructure systems. Cracks, delamination, and debonding change the strain field in these systems. Although conventional electromechanical sensors are commonly used for strain sensing, their size, temperature sensitivity, electromagnetic interference vulnerability, and strong signal drift hampers

their application for many engineering applications.^[3] There has been a significant interest in deploying newer embeddable technologies for direct strain measurements, in particular fiber optic sensors.^[4–8] However, the sensing accuracy of the fiber optic sensors is usually affected by spatial resolution.^[9] In addition, these sensing modules are not cost-effective and involve time-consuming installation and protection procedures. Piezoelectric sensors have been recently gaining more tractions in the SHM field.^[10–14] Using piezoelectric sensors for large-scale SHM is not an economic approach.^[15] The surface charge of piezoelectric transducers produced by an applied force might be neutralized easily by charges from other resources, for example, airborne charges and current leakage.^[16] Therefore, the piezoelectric sensors may act as a high-pass filter for input signals, impeding pure static measurements. Temperature sensitivity of the piezoelectric sensors is another concern to be considered. The development of multifunctional self-sensing structural components can be an efficient approach to address the challenges associated with the current sensing techniques. In this context, fiber-reinforced polymers (FRPs) are arguably a viable option because of their massive utility in construction.^[17–22] FRPs have been widely used as a promising composite material with other integral sensing technologies.^[8,23–28] Wang et al.^[27] utilized carbon nanofibers to modify carbon FRP laminates. The change of electrical resistance of the laminates was monitored to detect the damage. Feng et al.^[26] integrated

Q. Zhang, K. Barri, A. H. Alavi
Department of Civil and Environmental Engineering
University of Pittsburgh
Pittsburgh, PA 15260, USA
E-mail: alavi@pitt.edu

S. R. Kari
Department of Electrical and Computer Engineering
University of Pittsburgh
Pittsburgh, PA 15260, USA

Z. L. Wang
School of Materials Science and Engineering
Georgia Institute of Technology
Atlanta, GA 30332, USA

Z. L. Wang
Beijing Institute of Nanoenergy and Nanosystems
Beijing 101400, China

A. H. Alavi
Department of Computer Science and Information Engineering
Asia University
Taichung, Taiwan

A. H. Alavi
Department of Bioengineering
University of Pittsburgh
Pittsburgh, PA 15260, USA

 The ORCID identification number(s) for the author(s) of this article can be found under <https://doi.org/10.1002/adfm.202105825>.

DOI: 10.1002/adfm.202105825

the piezoceramic transducers with the carbon FRP fabric attached to the concrete surface for damage detection. However, these FRP-based systems naturally inherit the limitations of the accompanying sensing modules. Providing a reliable external power resource for taking measurements is another drawback of these methods. Recently, there has been a growing interest in developing self-powered sensing and monitoring methods for civil infrastructure systems. Nearly all of the current studies have been using piezoelectric materials as their energy harvesting component.^[29] In addition to the aforementioned limitations of the piezoelectric materials, their output voltage signals are relatively small and vulnerable to environmental noises.^[7] Piezoelectric transducers are more suitable for high-frequency vibration application, which is usually beyond the operation frequency of civil infrastructure systems, that is, <10 Hz. Triboelectric nanogenerator (TENG) is proved to be a promising technology for mechanical energy harvesting.^[30–34] The concept of TENG was first introduced by Wang et al.^[35] TENGs produce electrical output based on triboelectrification and electrostatic induction in response to external mechanical stimulations.^[36–42] They can be utilized as active sensors via directly correlating the generated electrical signal with the mechanical triggering. TENG-based sensors can use the generated electric signal to self-power themselves as well.^[43,44] **Figure 1** shows the typical energy density for different types of currently available energy harvesting modalities (research projects and commercial devices).^[30,45–47] The current volume power density of TENGs has reached 490 kW m^{-3} ,^[30] while the highest reported volume power density of piezoelectric materials is 4 kW m^{-3} .^[47] Despite the remarkable advantages of TENGs over other comparable technologies, there are very limited studies in the area of deploying them for SHM systems.^[38,48–50] These studies merely use TENGs as external point sensors for localized vibration monitoring on structures. In this context, creating a new class of structural elements with built-in TENG systems for distributed sensing and energy harvesting is likely to be the next technological revolution in the SHM of the America's aging infrastructure systems.

Here, we present the striking concept of multifunctional TENG-enabled structural elements (TENG-SEs) with sensing and energy harvesting functionalities for multiscale distributed SHM. Without loss of generality, we demonstrate the capacity of this concept to create a new generation of self-sensing and self-charging composite reinforcement rebars. To achieve this

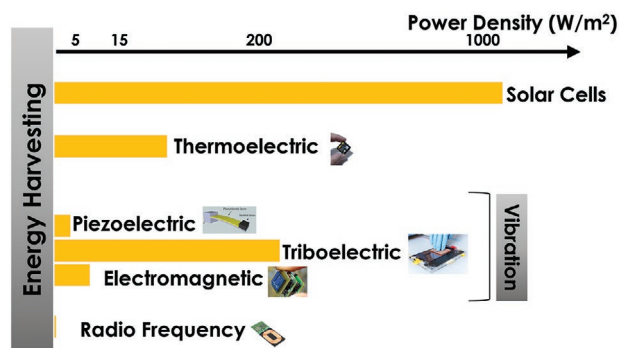


Figure 1. Power density for different available energy harvesting modalities.^[30,45–47]

goal, we introduce the TENG mechanisms into the fabrication process of the reinforcement rebars. We perform experiential and theoretical studies to verify the electrical and mechanical performance of the developed composite systems. The beauty of this concept is that the TENG-enabled rebars serve as both classical reinforcement systems for concrete structures and as a network of fully embeddable sensor-nanogenerators. In contrast to other competing technologies (e.g., piezoelectric materials, electromagnetic generators), the TENG-SEs can operate at low frequencies (<5–10 Hz), which is a major advantage for harvesting energy from civil infrastructure systems. We show the performance of the proposed systems for spatial sensing to detect any sign of structural damage at early stages. We discuss the capacity of these scalable and cost-effective sensing networks in transforming the SHM landscape for large-scale projects. We discuss how this concept could open the doors for widespread application of TENGs in civil infrastructure and construction fields, where TENG-enabled structural elements utilize merely their constituent components for sensing and energy harvesting purposes.

2. Results and Discussion

We demonstrate the first-of-its-kind integration of TENG mechanisms into the design process of structural elements for a broad range of civil infrastructure systems. **Figure 2a** presents our vision toward developing multifunctional TENG-SEs for distributed monitoring and energy scavenging at multiscale. TENG-SEs can be actively used to detect any sign of damage while providing enhanced mechanical performance due to their composite structure with tunable mechanical properties. The challenge would be how to integrate the TENG process into the texture of such elements. We investigate a major application area for the proposed technology by creating proof-of-concept reinforcement rebar prototypes. The reason behind this choice is that reinforcement rebars are currently used in nearly all of the large-scale concrete structures. **Figure 2b** shows the layered structure designed for the proposed proof-of-concept multifunctional FRP rebar according to the working principle of the TENGs systems. **Figure 2c** shows typical materials that can be used for fabricating the rebar layers. As seen, the smart FRP rebar consists of five layers. The core layer is a stiff carbon-fiber-reinforced polymer (CFRP) rod. An exterior layer is included to protect the internal layers against harsh construction conditions. This layer also protects the integrity of the entire system. Depending on the application environment, different types of materials can be used for designing the protection layer. Furthermore, this layer can be coated with commercially available rebar epoxies and chemical adhesives to protect the TENG-SEs against corrosion. The three interior layers (metal 1, dielectric, and metal 2) shown in **Figure 2a** create a built-in TENG system. TENGs have four fundamental working modes: vertical contact-separation mode, lateral sliding mode, single-electrode mode, and freestanding triboelectric-layer mode.^[44] The vertical contact-separation mode is considered in this study to develop the composite TENG rebars. In this mode, the physical contact of two different materials' surfaces with distinct electron affinity creates oppositely charged surfaces. A potential drop is created when two surfaces are

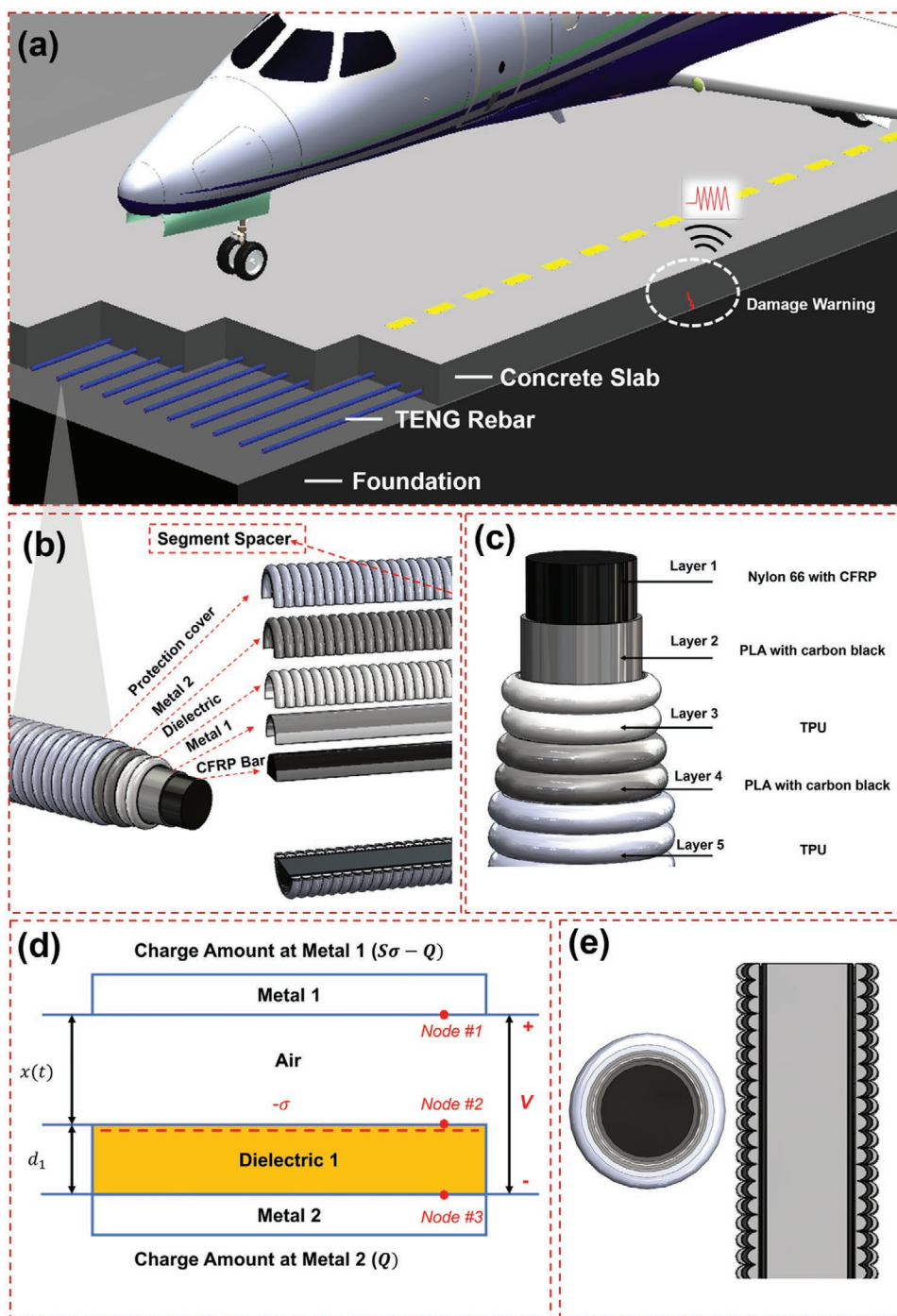


Figure 2. a) Multifunctional TENG-enabled structural elements used as reinforcement rebars in a concrete structure. b) Structure of the multifunctional TENG rebar. c) Typical materials used for fabricating the rebar layers. d) Theoretical model for conductor-to-dielectric attached-electrode parallel-plate contact-mode TENG. Reproduced with permission.^[53] Copyright 2014, Nano Energy. e) Top-view and side-view cross-section of smart rebar.

separated by a gap. Free electrons in one electrode would flow to the other electrode in order to balance the electrostatic field when the two electrodes are electrically connected by a load. The potential drop created by triboelectric charges disappears when the gap is closed, and the induced electrons will flow back.^[51,52]

An AC output is created due to this flow back and forth of electrons between the two electrodes.

The model for conductor-to-dielectric type is used here (Figure 2d). In this model, metal 1 is the top triboelectric layer as well as the top electrode, dielectric 1 with thickness d_1 is

the bottom triboelectric layer, metal 2 is the bottom electrode. The distance $x(t)$ between two triboelectric layers can be varied under external mechanical force. The inner surface of two triboelectric layers will have opposite static charges with an equal density of σ when they are in contact with each other under forces. The potential drop (V) between two electrodes will be induced when two triboelectric layers separate from each other with increasing x . The amount of transferred charges between the two electrodes, as driven by the induced potential, is Q . The total amount of charges in metal 1 can be defined as the sum of triboelectric charges ($S \times \sigma$), where S is the metal area size, and transferred charges $-Q$, namely $(S\sigma - Q)$. The amount of charges on metal 2 is Q . In the proposed design, segment spacers can be placed in metal 2 to divide the smart rebar into several segments for localized strain monitoring. Signal generated by each segment will be independent and only correlates to local structure conditions. This way, the entire smart rebar could also serve as multi-TENG segments, where the voltage generated by each TENG module reveals the local strain condition. Protection cover, metal 2, and dielectric layers are bonded together to be named as the “cloth”, metal 1 and CFRP rod is bonded together to be named as the “core” in rest of sections of this paper. The core is mechanically contacted with the cloth shown in Figure 2a. The cloth is designed to have a curvy structure inspired from ref. [54]. This curvy design helps achieve a larger separation between the cloth and core under tensile loading and provides better bonding with concrete. As shown in Figure 2b, Poly(lactic acid) (PLA) with carbon black (Young’s modulus $E = 3000$ MPa, Poisson’s ratio $\nu = 0.48$) was used for layer 2 and layer 4 to be the conductive layer. Thermoplastic Polyurethane (TPU) ($E = 26$ MPa, $\nu = 0.25$) was selected for layer 3 and layer 5 to be the dielectric layer and protection cover, respectively. Considering the requirement of mechanical properties for FRP reinforcement rebar and printing limitation of 3D printers, Nylon 66 with 10% carbon fiber reinforcement ($E = 7630$ MPa, $\nu = 0.35$) was used for layer 1. Figure 2e shows the top-view and side-view cross-section of the smart rebar. Under tensile loading scenario, the smart rebar work as a contact-separation TENG system. The working principle for smart rebar is schematically shown in Figure 3. At the initial state, the cloth is mechanically in contact with the core. After applying tensile loading, the cloth has larger elongation than the core due to the major stiffness differences. Then, the cloth starts separating from the core due to their different Poisson’s ratios. In the separated area between the core and the cloth, the cloth has a lower electric potential than the core, which produces a difference in electric potential by driving the electrons through the external tensile loads. After the tensile loads are removed, the cloth self-recovers to its initial position. In this stage, the gap will be closed. Subsequently, the potential drop created by triboelectric charges disappears and the induced electrons will flow back.

To test the functionality of the TENG rebar, experimental and theoretical studies were conducted. A series of uniaxial tension tests were first performed on the smart rebar prototypes. Three-point bending tests were then carried out on the reinforced concrete beam with embedded TENG rebars to evaluate the efficacy of the proposed system for damage detection. A 300 mm rebar with 25 mm diameter and 3 equal sensing TENG segments was 3D printed and tested. Figure 4

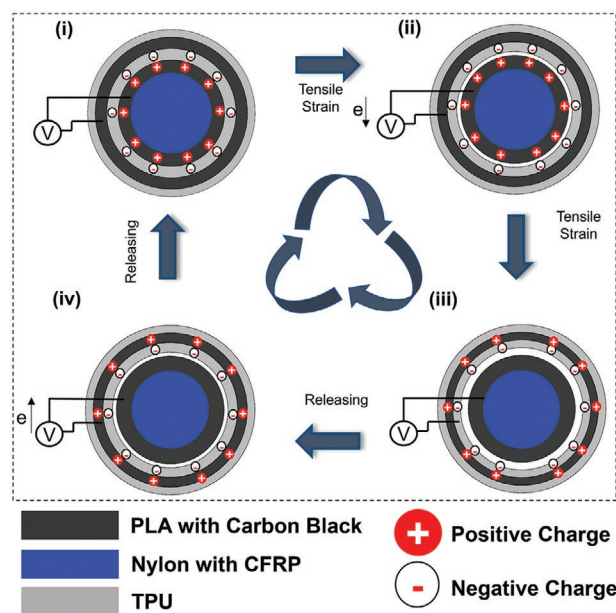


Figure 3. Electrical energy generation process of the multifunctional TENG rebar under tensile loading.

shows the 3D printing process, printed prototype, test setup, and the triboelectrification process within the smart rebar. Displacement controlled cyclic tests with maximum strain equals 1% and 2% were conducted, respectively. The position and loading amplitudes were recorded. A video showing the typical voltage signal generated by the three-segment TENG rebar under tensile loading is provided in the Supporting Information. Figure 5a–d presents a comparison of the measured and theoretical voltage values during the tensile tests and the corresponding loads for 1% and 2% strain levels. Details of the theoretical model are described in Materials and Methods. As seen, the voltage is proportional to the applied displacement and accordingly to the strain induced in the TENG rebar. In addition, there is an acceptable agreement between the experimental and theoretical results. The results imply the feasibility of creating a self-power and self-sensing rebars via integrating contact-electrification into their fabrication process. Figure 5e–h illustrates the smart rebar charging characteristics under periodical mechanical motion with 2% strain. Figure 5e shows the current generated by the TENG rebar under the applied loading cycles. Figure 5f,g show the changes of voltage and stored charge for different load capacitances, respectively. At $t = 0$, the charging speed is maximum, and it gradually decreases over time. The saturation voltage is about 1.4 V. Figure 5h shows the variations of voltage, stored charge against capacitance, and the associated error bars at 40 s.

To further evaluate the damage detection performance of the proposed smart rebar in concrete, a series of three-point bending tests were conducted at two different scales. Figure 6 shows the TENG rebars, concrete pouring process, test setup, and testing results. First, a single-segment smart rebar with 160 mm length and 20 mm diameter was printed. The rebar was cast into a small concrete beam with 210 mm length and 25.4 mm by 25.4 mm cross-section (Figure 6c). In the second testing phase, a two-segment smart rebar with 200 mm length

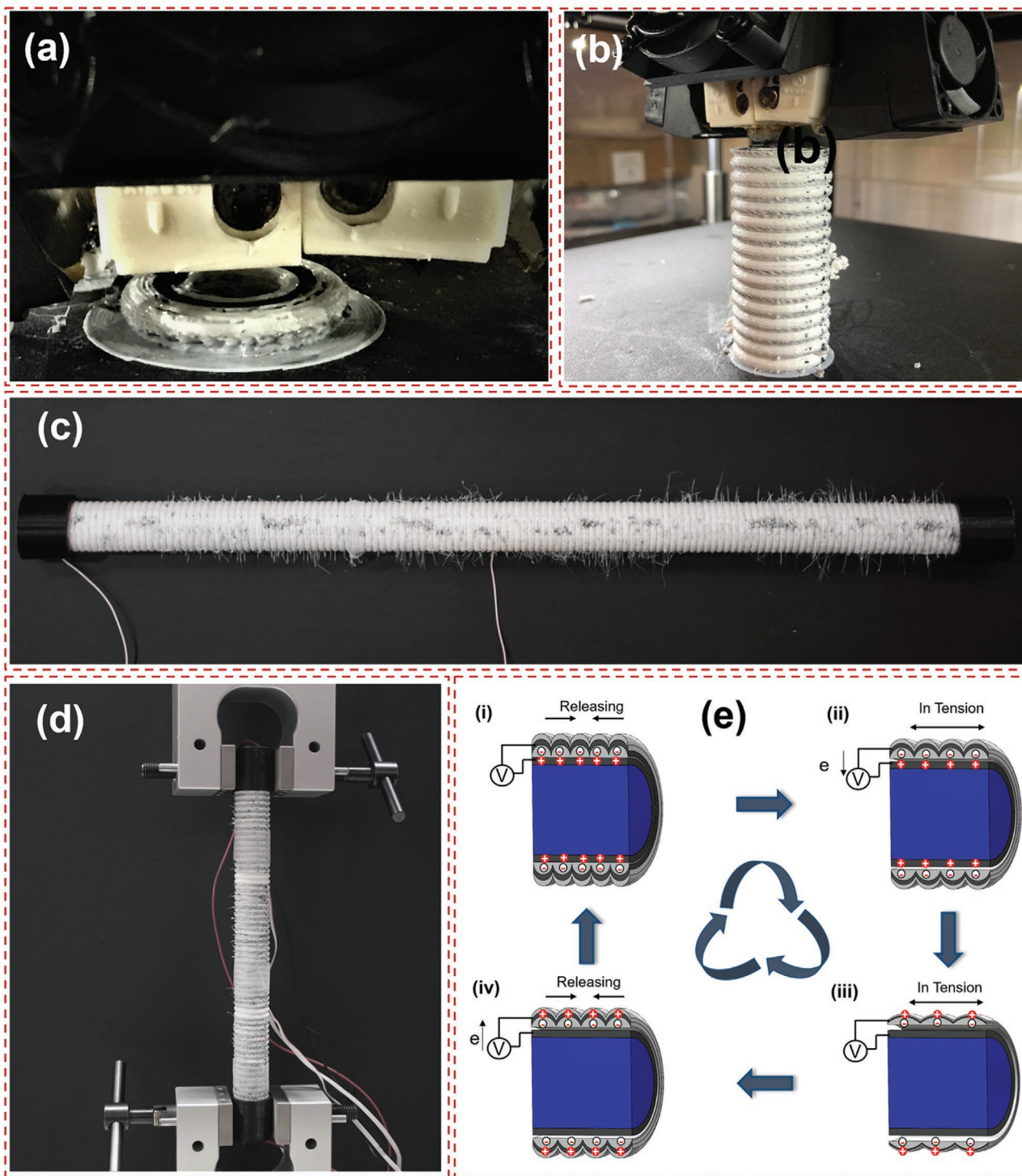


Figure 4. a,b) 3D printing process of the smart TENG rebar. c) Fabricated prototype. d) TENG rebar under cyclic tensile testing, e) Triboelectrification process occurring within the smart rebar components.

and 25 mm diameter for each segment was printed and cast into a larger concrete beam with 420 mm length and 152 mm by 152 mm cross-section (Figure 6d). It is well-known that the operation frequency of most of the civil infrastructure systems is low (<10 Hz) denoting a quasi-static condition. TENGs are most effective for the detection of dynamic changes in struc-

tures. In order to assess the efficacy of the TENG rebars in detecting slow and quasi-static changes in structures, displacement control three-point bending tests were conducted on both beams with small cyclic loading frequency of 0.5 Hz. Figure 6e shows the voltage generated by the entire piece of the TENG rebar embedded inside the small-scale sample.

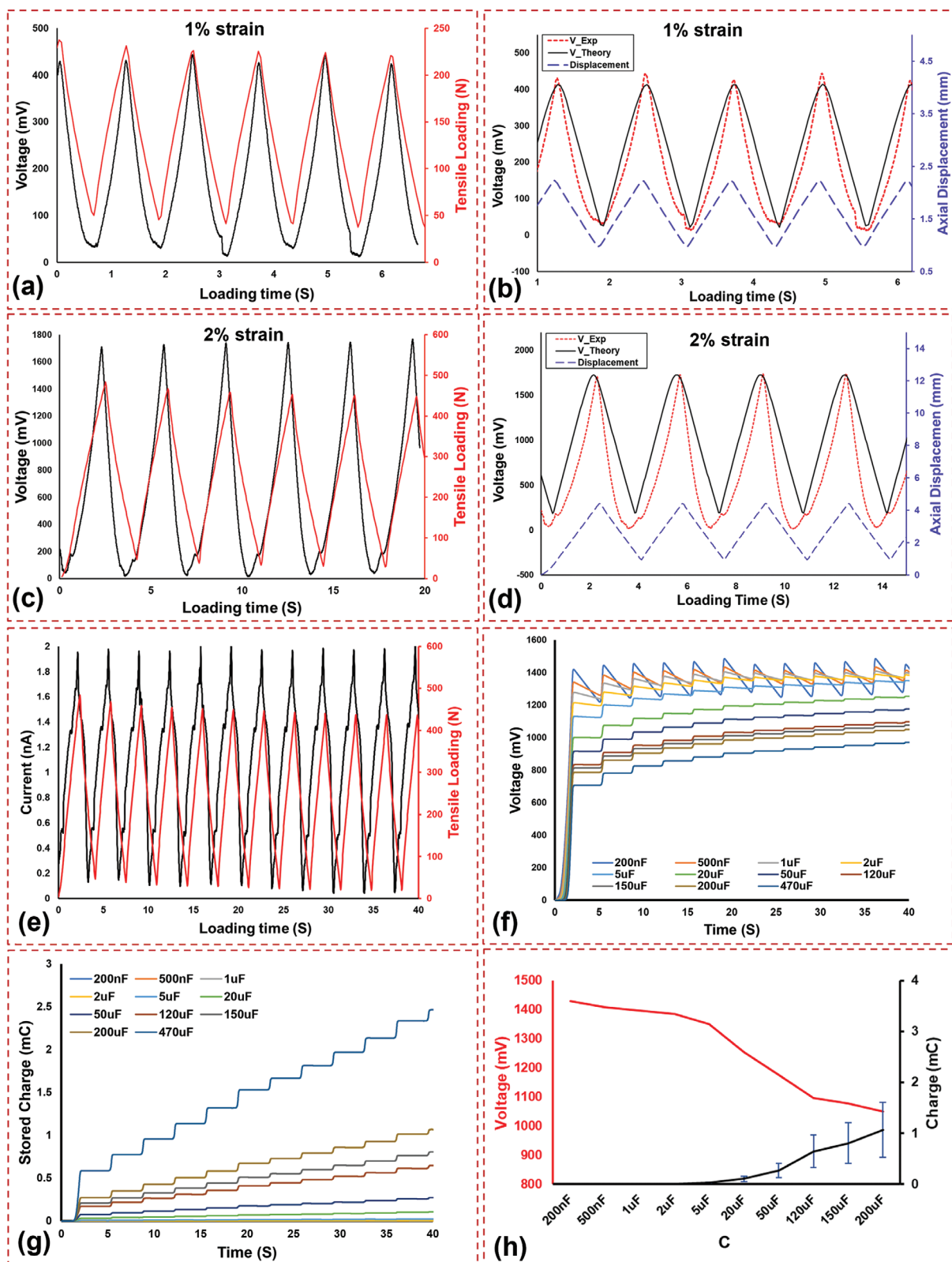


Figure 5. a) Tensile loading and corresponding voltage generated by the TENG rebar for 1% strain. b) Measured and theoretical voltage for 1% strain. c) Tensile loading and corresponding voltage generated by the TENG rebar for 2% strain. d) Measured and theoretical voltage for 2% strain. e) Current generated by the TENG rebar for 2% strain. Charging diagrams showing f) Voltage changes at different load capacitances for 2% strain. g) Stored charge changes at different load capacitances for 2% strain. h) Variations of the stored voltage and charge against capacitance at 40 s.

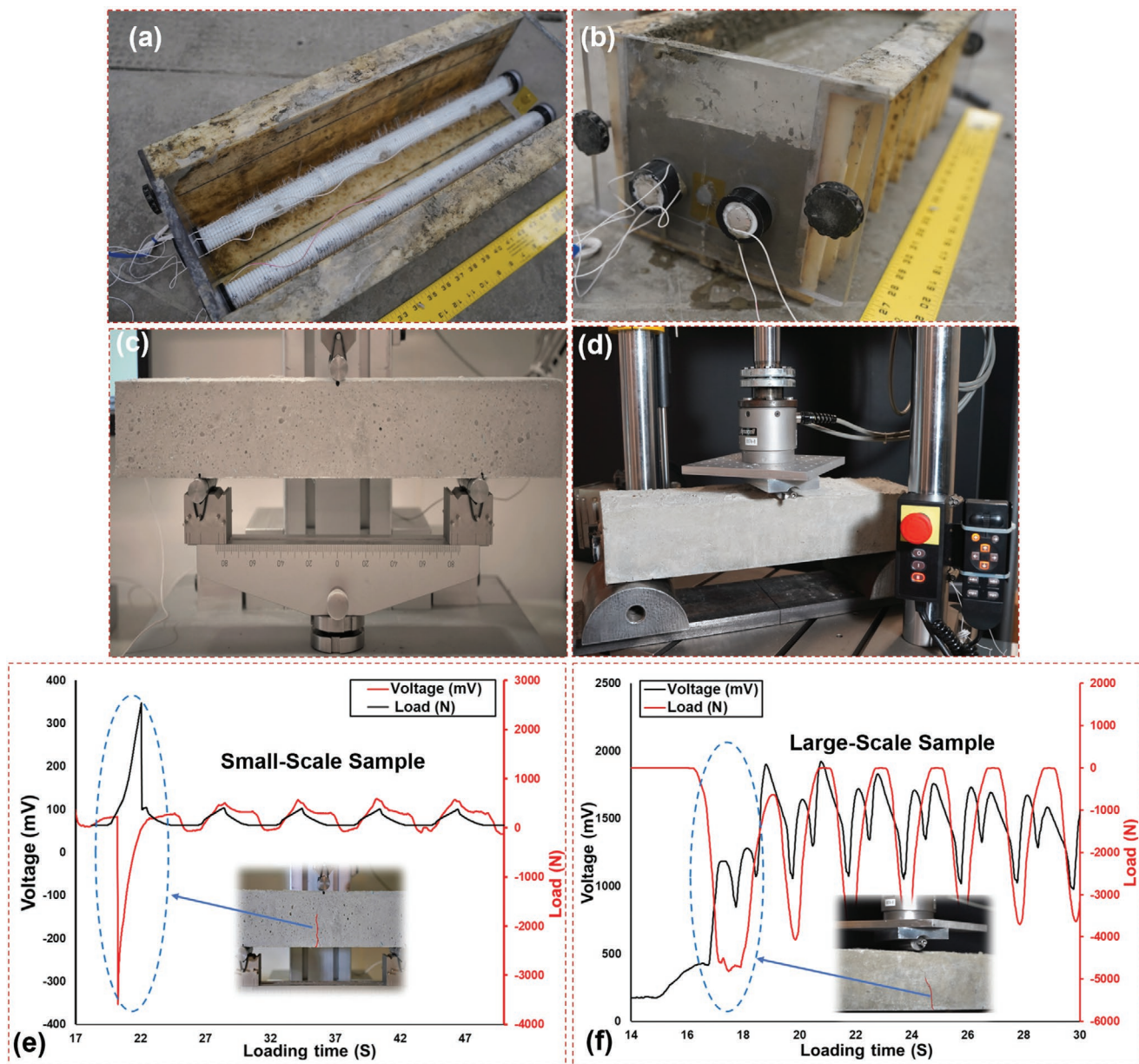


Figure 6. a,b) Fabricating the concrete beams with embedded TENG rebars. c) Test setup for the small-scale concrete beam, d) Test setup for large-scale concrete beam. TENG rebar voltage signal during loading, crack initiation, and crack propagation: e) Small-scale concrete beam. f) Large-scale concrete beam.

Figure 6f shows the voltage generated by one of the segments of the rebar in large-scale sample. Referring to these figures, the TENG rebars are capable of harvesting energy from the low-frequency mechanical excitations. A sharp increase was observed in the generated voltage when cracking occurred at the bottom of the beams. For small-scale concrete beams, crack happened with 1 mm displacement. For large-scale concrete beam, crack initialized under 2 mm displacement. With continuous loading after crack initialization, the rebar was bearing cyclical tension loading. In this phase, the voltage signal became periodical and stable. As shown in Figure 6d,e, peak to peak voltage values were 70 and 750 mv for the small

and large-scale concrete beams, respectively. According to the results, the smart rebars act as reinforcement to prevent the collapse after damage is initialized. The sharp increase in voltage can be considered as a reliable damage initialization alarm. Thereafter, the progression of damage can be continuously monitored by tracking the changes of the TENG rebar voltage amplitudes with respect to a baseline in the post-damage period. It is worth mentioning that standard steel rebars have been dominating the construction industry for decades. Corrosion of reinforcing steel rebars has been the leading cause of deterioration in concrete systems. In addition to corrosion, there are many other issues associated

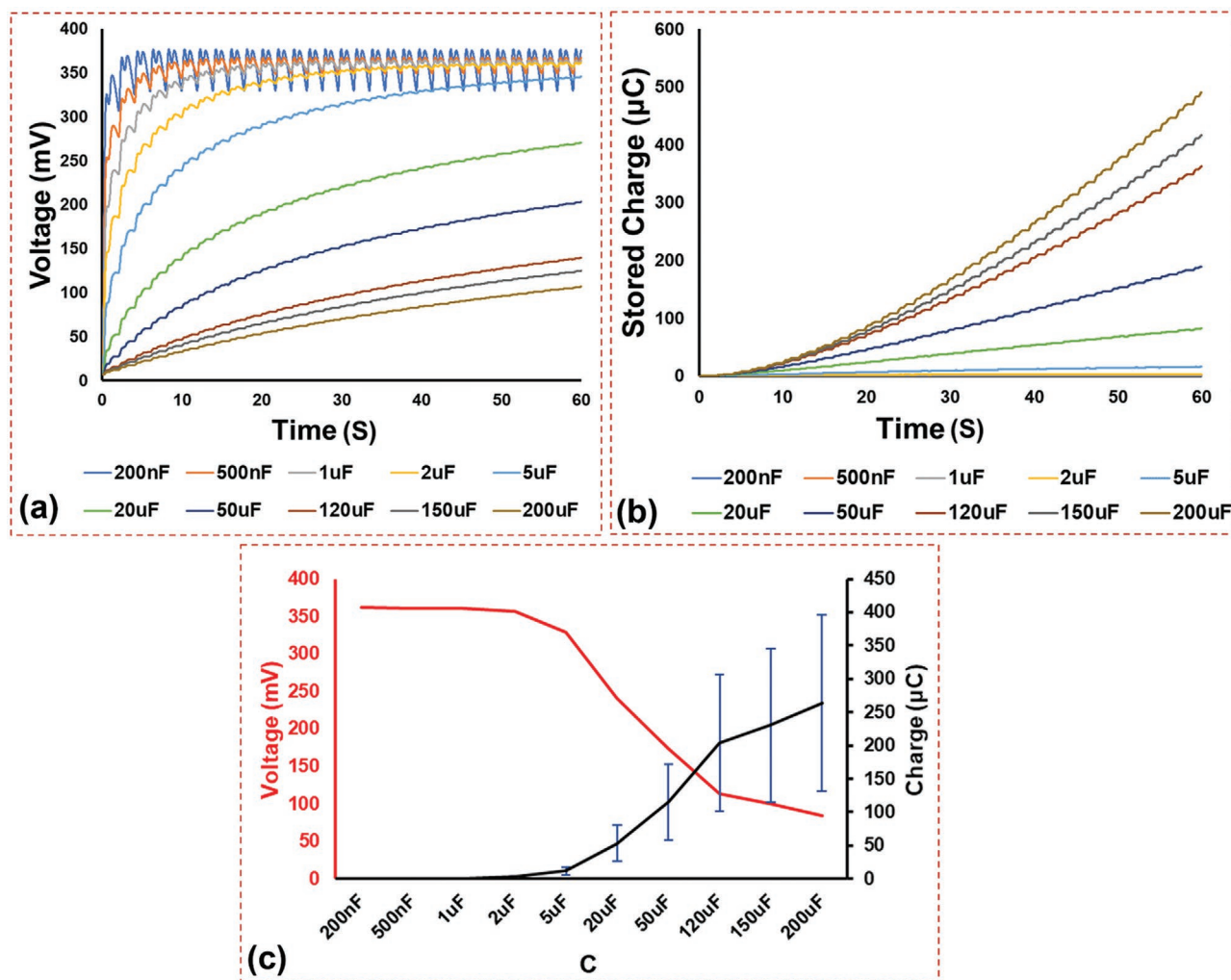


Figure 7. Charging diagram for large-scale concrete sample after crack initiation. a) Voltage changes at different load capacitances. b) Stored charge changes at different load capacitances. c) Variations of the stored voltage and charge against capacitance at 40s.

with using standard steel rebars such as their high stiffness and limited fatigue resistance. Composite rebars including CFRPs are proved to be extremely strong and light compared to steel rebars.^[55] They are now being widely used as corrosion-resistant alternatives to steel reinforcement in concrete structures susceptible to corrosion fields and structures under extreme environments.^[55] A TENG-SE rebar is naturally a composite CFRP rebar that would inherit these important properties. **Figure 7** illustrates the charging characteristics of the proposed TENG-SE CFRP rebar under cyclic three-point bending for the large-scale concrete sample after crack initiation. The voltage and the stored charge variations at different load capacitances are shown in Figure 7a,b. As seen in Figure 7a, the low capacitance capacitors are charged rapidly and immediately reach saturation voltage. While for capacitors with higher capacitance, saturation occurs more slowly. The saturation voltage is approximately 370 mV. Referring to Figure 7b, the measured maximum pick-to-pick voltage is 750 mV. Therefore, the saturated voltage is nearly half of the maximum measured voltage. Figure 7c shows the effect of

capacitance on the voltage and charge stored in the capacitors after 40 s.

The prototypes presented in this study are proof-of-concept designs to demonstrate the first application of TENG-SEs for sensing and monitoring of large-scale civil infrastructure systems. The prototypes were not optimized for the best mechanical and electrical performance. In fact, these performance indexes should be customized for any TENG-SE system according to the design requirements for the investigated civil engineering structure and the anticipated loading levels and traffic vibrations applied to the structure. Taking into account the high power density of TENGs ($>490\text{ kW m}^{-3}$) as reported in previous studies,^[30,47] it is reasonable to expect that task-specific and problem-customized TENG-SEs could achieve high output area power density and instantaneous conversion efficiency. Depending on the target application area, a number of robust material and surface optimization approaches (e.g., refs. [51,56–58]) can be used to tune the electrical and mechanical performance of the TENG-SE systems. Since TENG-based systems offer high output voltage but low output current, they

should be integrated with power management circuits with high efficiency for energy harvesting tasks.^[59–61] However, the results presented in this study highlight the significant potential of the TENG-SEs in pushing the limits of SHM. The TENG-enabled elements can be embedded within large structural systems to harvest the energy from traffic vibrations, which normally have frequencies ranging from 1 to 250 Hz.^[62] In this operational modal analysis (OMA), the same signal harvested by the TENG element from the traffic loading can be used for monitoring the structural condition. The tension reinforcement TENG-SEs can serve best for large-scale distributed sensing in case they are buried inside concrete structures. This is because the harvestable mechanical vibrations within the tension zone in concrete structures are not usually significant. In this case, the TENG-SEs can be interfaced with low-power consumption electronics such as low-power wireless data logging technologies to create fully self-powered systems without a need for additional electronics. As an example, the TENG-SE signal can be readily used to empower a self-powered floating-gate data logger (power consumption < 150 Nanowatts)^[63,64] or Fowler–Nordheim (FN) sensor-data-logger (power consumption < 100 femtowatts).^[65,66] This way, the integrated TENG element and data-logger can potentially record all events and aggregate the short-term fluctuations. Any change in signal patterns in the long term can be correlated with the condition degradation. The data continuously stored by the data-logger can be read using passive or semi-active radio frequency (RF) readers mounted on vehicles or unmanned aerial vehicles. On the other hand, for exposed structural systems (e.g., bridge gusset plates) with large amplitude mechanical vibrations,^[63] the TENG-SEs cannot only serve as a sensing medium but can also harvest a significant amount of energy.

Furthermore, the standard nondestructive evaluation (NDE) approaches can be coupled with TENG-SEs to assess the progression of damage via an experimental modal analysis (EMA). In the EMA-based method, impulse tests, based on the excitation of the structure using commonly-used vibration exciters or modal hammers, can be used to excite the TENG elements and evaluate the changes in the signal patterns due to damage progression. A drawback of the EMA approach is that the structural health state is evaluated only as a snapshot in time where the measurements are taken. However, compared to standard NDE methods, TENG elements can be used for both local and distributed sensing. The NDE methods can only be used for damage localization of surface and subsurface defects. Embeddable TENG elements cannot only perform these tasks continuously and in real-time but can also detect bottom-up cracks which are difficult, if not impossible to assess. Although we showed the capacity of the TENG-SEs for strain sensing, the designs can be readily modified to serve as a shear sensor. Measuring contact shear at the interface surface is a difficult task. Complicated electroding methods and challenges in evaluating the performance of piezoelectric sensors operating in the shear mode have remarkably limited their practical use.^[67] Using the TENG lateral-sliding and freestanding triboelectric-layer modes in the fabrication of structural elements would make it feasible to measure the shear forces applied to the slider in the direction of sliding through the generated voltage. In fact, the relative sliding motion between the two different bonded materials

gives rise to a triboelectric charge that is picked up by the electrodes and is proportional to the shear stress. Measuring actual contact shear at the interface surface within the unexplored structural response range of <10 Hz can potentially lead to new concepts and mechanisms in the fields of aerospace, medical, civil infrastructure, and construction. Since such a sensing system would be intrinsically sensitive to shear stress, it can as well be implemented in various other materials or structures such as polymer or composite materials. Some application examples are built-in diagnostics of inter-laminar shear stress of composite structures, wall shear stress measurements, monitoring shear stresses in concrete structures, monitoring shear stresses in large structures, etc.

Arguably, successful development of the proposed TENG-SEs concept and installation procedure could dramatically transform the economics of transportation infrastructure preservation/management and ultimately improve the serviceability of these systems. This is a paradigm shift technology and has unprecedented performances. Such scalable and cost-effective network can not only be used for discrete and localized sensing but also for spatial structural sensing. A TENG sensing network can be embedded at the interface of structural layers and serve as a large-scale and low-cost flexible self-powered sensing skin distributed over the structure. TENGs have been already used as tactile sensing arrays for robots to detect physical contact with humans or environment.^[68] When embedded inside the civil infrastructure systems, the envisioned TENG sensing skin can create a multifunctional digital surface element capable of performing multiple functions (**Figure 8**). A TENG sensing skin can serve as a living structure responding to its environment and self-monitoring its condition. Furthermore, this smart sensitive skin can be potentially used for: 1) generating energy required for built-in smart signage technologies, navigational beacons and other embedded infrastructure sensors, 2) vehicle-to-infrastructure (V2I) communication, in particular communicating with and charging autonomous vehicles (AVs), and 3) enabling a proxy weigh-in-motion system to assess the weight of vehicles traveling over the pavement.

3. Conclusion

In summary, a novel concept of self-sensing and self-powering TENG-SEs was proposed in this study. We leveraged advances in structural engineering and the TENG-based sensing mechanism to introduce new aspects of multifunctionality into the fabric of civil infrastructure systems. We fabricated proof-of-concept prototypes to demonstrate the feasibility of the proposed approach for large-scale health monitoring of the structures. The proposed systems offer unique functionality in distributed sensing which has been a major challenge for mega-size projects. The experimental and theoretical results confirm the efficiency of the TENG-SEs in detecting damage and harvesting energy from mechanical excitations. A series of promising tests with segmented TENG rebars embedded in concrete beams reveal that the proposed concept can also be used for damage localization and energy harvesting. Various TENG modes can be introduced to design structural elements

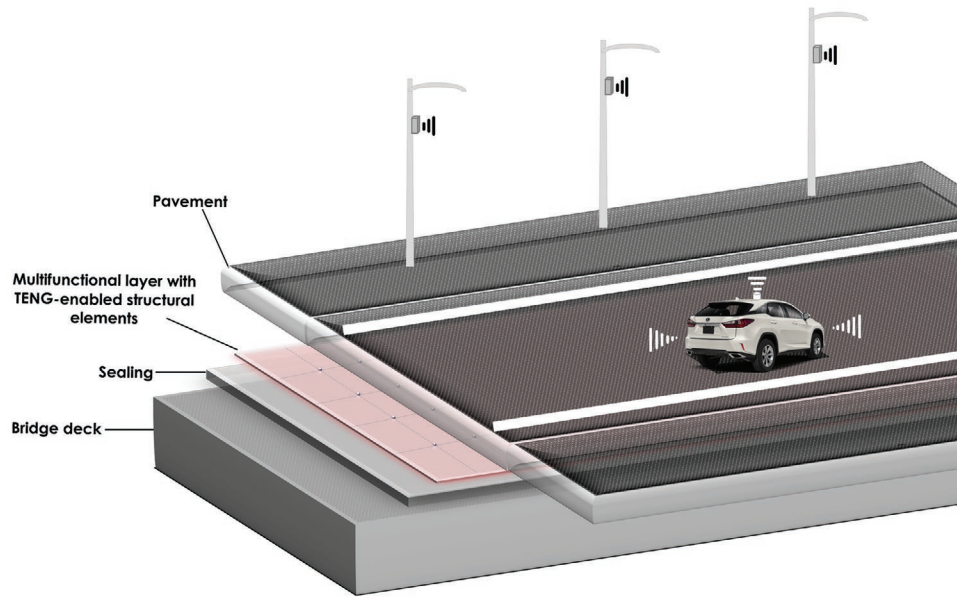


Figure 8. A conceptual representation of a smart and multifunctional layer with TENG-SEs which can be embedded in bridge deck pavement to perform multiple tasks including SHM, V2I communication, charging AVs, and other built-in embedded sensors, and a potential autonomous, battery-free weigh-in-motion system.

with different sensing modalities. The observations imply that the proposed concepts could open an avenue for the next stage of the revolution in SHM where a new generation of scalable, cost-effective, and multifunctional sensor-nanogenerator structural elements could be widely used for real-time assessment and empowering of our aging civil infrastructure systems. These features eliminate the need for massive networks of power-hungry sensors attached to or embedded inside the structures.

4. Experimental Section

Fabrication of the TENG-Enabled Structural Elements at the Multiscale: In this study, the TENG-enabled rebar prototypes were fabricated using Raise3D Pro2 Dual Extruder 3D Printer. First, 3D models of the designs were created using SolidWorks. The dual extruder 3D printer was then used to fabricate the samples. The prototypes were ready for being tested immediately because their layers were simultaneously printed. The material used for fabricating the concrete beams was cement paste, a basic mixture of Type I/II Portland cement and water. Water to cement ratio was 0.45. Samples were wet cured for 28 days.

Electrical Measurement and Characterization: The uniaxial loading tests were carried out on the rebar samples using a TestRecources Universal Testing Machine. For the tension tests, a set of anchors were printed with PLA and used to ensure the uniform tensile loading at both ends. The concrete beams with embedded TENG rebars were tested using an Instron Testing Machine (Model 8874). There were various reliable methods to measure the voltage of a TENG system (e.g., refs. [69,70]). In this study, an NI 9220 module (1 GΩ impedance) was used to read the TENG rebar voltage. An SR570 low-noise current amplifier device by Stanford Research Systems was used for current measurements. The measurements were controlled using a LabVIEW program.

Electrical Characterization: In the proposed smart TENG-enabled rebar, the thickness of the dielectric layer is d_1 , and the relative dielectric

constant is ϵ_{r1} . The dielectric layer equivalent thickness (d_0) can be written as:

$$d_0 = \frac{d_1}{\epsilon_{r1}} \quad (1)$$

the V-Q-x relationship is expressed as:^[57]

$$V = -\frac{Q}{S\epsilon_0} [d_0 + x(t)] + \frac{\sigma x(t)}{\epsilon_0} \quad (2)$$

where $x(t)$, S , σ , and ϵ_0 denote the varying gap distance, effective contact area, charge density, and vacuum permittivity, respectively. Since the cyclic loading applied to the proposed TENG rebar was displacement-control, the strain in the longitudinal direction can be calculated as:

$$\epsilon_{11} = \frac{\Delta y}{y} = \frac{y(t)}{L} \quad (3)$$

where $y(t)$ is the elongation in the longitudinal direction and L is the total length of the testing sample.

Assuming the tensile loading was uniformly applied to surfaces of both ends and it was in cylindrical shape, this problem can be solved as a 2D finite element problem under plane stress conditions.^[71] Therefore, the transverse strain can be calculated based on the equation of Poisson's ratio:

$$\nu = \frac{\epsilon_{22}}{\epsilon_{11}} \quad (4)$$

$$\epsilon_{22} = \epsilon_{11} \nu = \frac{y(t)\nu}{L} \quad (5)$$

Since the cloth consists of two materials, the Poisson's ratio is defined as ν_{TPU} for layer 3 and 5, ν_{PLA} for layer 4.

$$x(t) = \left(\frac{d_{I3} + d_{I5} \nu_{TPU} + \frac{d_{I4}}{L} \nu_{PLA}}{L} \right) y(t) \quad (6)$$

where d_{cloth} is the thickness of the cover.

With the TENG rebar connected to a load resistance (R), the generated voltage V can be obtained as:

$$V = R \frac{dQ}{dt} \quad (7)$$

Where

$$\frac{dQ}{dt} = -\frac{Q}{S\epsilon_0 R} (d_0 + x(t)) + \frac{\sigma x(t)}{\epsilon_0 R} \quad (8)$$

This is a first-order ordinary differential equation and can be solved by specifying the boundary condition. Since the loading applied to smart rebar is in a constant velocity, the simplified equation for $Q(t)$, $I(t)$, and $V(t)$ are as below:^[57]

$$Q(t) = \sigma S \left[1 - \exp(-At - Bt^2) + \sqrt{2}F \exp(-At - Bt^2) \times \text{Dawson} \left(\frac{F}{\sqrt{2}} \right) - \sqrt{2}F \times \text{Dawson} \left(\frac{F}{\sqrt{2}} + \sqrt{Bt} \right) \right] \quad (9)$$

$$I(t) = \sigma S \left[\exp(-At - Bt^2)(A + 2Bt) - \sqrt{2}F \exp(-At - Bt^2)(A + 2Bt) \times \text{Dawson} \left(\frac{F}{\sqrt{2}} \right) - A + 2A \left(\frac{F}{\sqrt{2}} + \sqrt{Bt} \right) \times \text{Dawson} \left(\frac{F}{\sqrt{2}} + \sqrt{Bt} \right) \right] \quad (10)$$

$$V(t) = \sigma SR \left[\exp(-At - Bt^2)(A + 2Bt) - \sqrt{2}F \exp(-At - Bt^2)(A + 2Bt) \times \text{Dawson} \left(\frac{F}{\sqrt{2}} \right) - A + 2A \left(\frac{F}{\sqrt{2}} + \sqrt{Bt} \right) \times \text{Dawson} \left(\frac{F}{\sqrt{2}} + \sqrt{Bt} \right) \right] \quad (11)$$

where constants A , B , and F are defined as:

$$A = \frac{d_0}{RS\epsilon_0} \quad (12)$$

$$B = \frac{\nu}{2RS\epsilon_0} \quad (13)$$

$$F = \frac{A}{\sqrt{2}B} \quad (14)$$

The Dawson's integral ($\text{Dawson}(x)$) is shown as:

$$\text{Dawson}(x) = \exp(-x^2) \int_0^x \exp(y^2) dy \quad (15)$$

The contact area is the inner surface of the cover:

$$S = 2\pi rL \quad (16)$$

where r is the radius of the inner surface of the cloth. Theoretical voltage values are calculated with parameters listed in **Table 1**. These parameters have been recommended by Niu and Wang.^[53]

Table 1. Geometric and material properties of the TENG-enabled rebar.

Geometric properties [mm]	Cloth inner surface radius [mm]	r
Length of sample	L	B
Thickness of dielectric layer	d_1	d_1
Thickness of the layer 3	d_{I3}	d_{I3}
Thickness of the layer 4	d_{I4}	d_{I4}
Thickness of the layer 5	d_{I5}	d_{I5}
Material properties	Relative permittivity of the dielectric layer (TPU) ϵ_{r1}	7.2
Permittivity of vacuum ϵ_0		8.854×10^{-12}
Surface charge density σ [$C m^{-2}$]		20×10^{-6}
Load resistance R [Ohm]		7.5×10^{10}
	ν_{TPU}	0.48
	ν_{PLA}	0.25

Supporting Information

Supporting Information is available from the Wiley Online Library or from the author.

Acknowledgements

Research reported in this work was supported in part by the National Institute of Arthritis and Musculoskeletal and Skin Diseases of the National Institutes of Health under award number R21AR075242-01. A.H.A. acknowledges the startup fund from the Swanson School of Engineering at the University of Pittsburgh.

Conflict of Interest

The authors declare no conflict of interest.

Data Availability Statement

Data sharing is not applicable to this article as no new data were created or analyzed in this study.

Keywords

civil infrastructure, distributed sensing, energy harvesting, multifunctional structures, triboelectric nanogenerators

Received: June 16, 2021

Revised: July 23, 2021

Published online:

[1] B. Han, J. Ou, *Sens. Actuators, A* **2007**, *138*, 294.

[2] Q. Zhang, K. Barri, S. K. Babanajad, A. H. Alavi, *Engineering* **2020**, <https://doi.org/10.1016/j.eng.2020.07.026>.

[3] S. Sulejmani, C. Sonnenfeld, T. Geernaert, G. Luyckx, D. V. Hemelrijck, P. Mergo, W. Urbanczyk, K. Chah, C. Caucheteur, P. Mégret, H. Thienpont, F. Berghmans, *Opt. Express* **2013**, *21*, 20404.

[4] Z. S. Wu, B. Xu, H. Keiji, M. Atsuhiko, *Eng. Struct.* **2006**, *28*, 1049.

[5] W. Zhang, B. Shi, Y. F. Zhang, J. Liu, Y. Q. Zhu, *Smart Mater. Struct.* **2007**, *16*, 843.

- [6] B. Benmokrane, M. Quirion, E. El-Salakawy, *Nondestructive Evaluation and Health Monitoring of Aerospace Materials and Composites III*, Vol. 5393, San Diego, CA, USA **2004**, <https://doi.org/10.1117/12.548600>.
- [7] B. Benmokrane, A. Debaiky, A. El-Ragaby, *Proc. SPIE 6176, Nondestructive Evaluation and Health Monitoring of Aerospace Materials, Composites, and Civil Infrastructure V*, **2006**.
- [8] Y. Tang, Z. Wu, *Sensors* **2016**, *16*, 286.
- [9] H. Zhang, Z. S. Wu, *Struct. Health Monit.* **2008**, *7*, 143.
- [10] Y. Hu, H. Yang, *Smart Mater. Struct.* **2007**, *16*, 706.
- [11] Y. Yang, V. Annamdas, C. Wang, Y. Zhou, *Sensors* **2008**, *8*, 271.
- [12] W. H. Duan, Q. Wang, S. T. Quek, *Materials* **2010**, *3*, 5169.
- [13] X. Q. Zhu, H. Hao, K. Q. Fan, *J. Civ. Struct. Health Monit.* **2013**, *3*, 105.
- [14] K. Xu, Q. Kong, S. Chen, G. Song, *IEEE Sens.* **2017**, *17*, 3244.
- [15] R. Garland, *White paper*, Stanford University, Stanford, CA **2012**.
- [16] P. Regtien, E. Dertien, *Sensors for Mechatronics*, 2nd ed., Elsevier, **2018**, <https://www.elsevier.com/books/sensors-for-mechatronics/regtien/978-0-12-813810-6>.
- [17] J. Teng, J.-F. Chen, S. T. Smith, L. Lam, *FRP: Strengthened RC Structures*, Wiley, Hoboken, NJ, USA **2002**.
- [18] Y. Zheng, C. Li, J. Yang, C. Sun, *Compos. Struct.* **2015**, *132*, 20.
- [19] M. Luo, W. Li, C. Hei, G. Song, *Sensors* **2016**, *16*, 2083.
- [20] F. Nerilli, G. Vairo, *Composites, Part B* **2018**, *153*, 205.
- [21] B. Shadravan, F. M. Tehrani, *Period. Polytech., Civ. Eng.* **2017**, *61*, 740.
- [22] N. R. Abdelal, M. R. Irshidat, *Struct. Eng. Mech.* **2019**, *72*, 3050312.
- [23] L. Xia, Y. Zheng, *Appl. Sci.* **2018**, *8*, 721.
- [24] Y. Zheng, L. Zhou, L. Xia, Y. Luo, S. E. Taylor, *Eng. Struct.* **2018**, *171*, 500.
- [25] ACI Committee 440, *Guide for the Design and Construction of Structural Concrete Reinforced with Fiber-Reinforced Polymer (FRP) Bars*, American Concrete Institute (ACI), Farmington Hills, MI, USA **2015**.
- [26] Q. Feng, J. Ou, *Sensors* **2018**, *18*, 4137.
- [27] Y. Wang, R. Chang, G. Chen, *Adv. Mech. Eng.* **2017**, *9*, 1.
- [28] Y. Wang, Y. Wang, B. Wan, B. Han, G. Cai, R. Chang, *Composites, Part A* **2018**, *113*, 40.
- [29] H. Salehi, R. Borgeño, S. Chakrabarty, N. Lajnef, A. H. Alavif, *Eng. Struct.* **2021**, *234*, 111963.
- [30] Z. L. Wang, *ACS Nano* **2013**, *7*, 9533.
- [31] T. Quan, Z. L. Wang, Y. Yang, *ACS Appl. Mater. Interfaces* **2016**, *8*, 19573.
- [32] Y. Wang, Y. Yang, Z. L. Wang, *npj Flex Electron.* **2017**, *1*, 10.
- [33] W. Tang, T. Jiang, F. R. Fan, A. F. Yu, C. Zhang, X. Gao, Z. L. Wang, *Adv. Funct. Mater.* **2015**, *25*, 3718.
- [34] R. Wen, J. Guo, A. Yu, J. Zhai, Z. I. Wang, *Adv. Funct. Mater.* **2019**, *29*, 1807655.
- [35] F.-R. Fan, Z.-Q. Tian, Z. L. Wang, *Nano Energy* **2012**, *1*, 328.
- [36] X. Li, C. Jiang, Y. Ying, J. Ping, *Adv. Energy Mater.* **2020**, *10*, 2002001.
- [37] C. Jiang, X. Li, Y. Ying, J. Ping, *Nano Energy* **2020**, *74*, 104863.
- [38] C. Jiang, C. Wu, X. Li, Y. Yao, L. Lan, F. Zhao, Z. Ye, Y. Ying, J. Ping, *Nano Energy* **2019**, *59*, 268.
- [39] H. Yu, W. Ding, Y. Hu, D. Yang, S. Lu, C. Wu, H. Zou, R. Liu, C. Lu, Z. L. Wang, *Adv. Energy Mater.* **2017**, *7*, 1700565.
- [40] M. Ma, Q. Liao, G. Zhang, Z. Zhang, Q. Liang, Y. Zhang, *Adv. Funct. Mater.* **2015**, *25*, 6489.
- [41] Z. Su, M. Han, X. Cheng, H. Chen, X. Chen, H. Zhang, *Adv. Funct. Mater.* **2016**, *26*, 5524.
- [42] K. Chen, L. Zhang, X. Kuang, V. Li, M. Lei, G. Kang, Z. L. Wang, H. J. Qi, *Adv. Funct. Mater.* **2019**, *29*, 1903568.
- [43] Z. L. Wang, *Mater. Today* **2017**, *20*, 74.
- [44] Z. L. Wang, J. Chen, L. Lin, *Energy Environ. Sci.* **2015**, *8*, 2250.
- [45] D. Jourdan, *MEMS energy harvesting devices, great technology: For which markets?*, Micronews, **2008**, <https://perso.esiee.fr/~bassetp/fichiers/mn73oct2008.pdf>.
- [46] B. Dziadok, Ł. Makowski, A. Michalski, *Metrol. Meas. Syst.* **2016**, *23*, 495.
- [47] S. S. Indira, C. A. Vaithilingam, K. S. P. Oruganti, F. Mohd, S. Rahman, *Nanomaterials* **2019**, *9*, 773.
- [48] S. Li, D. Liu, Z. Zhao, L. Zhou, X. Yin, X. Li, Y. Gao, C. Zhang, Q. Zhang, J. Wang, *ACS Nano* **2020**, *14*, 2475.
- [49] A. M. Nazar, K.-J. I. Egbe, P. Jiao, A. H. Alavi, in *American Professional Society of Photographic Instrumentation Engineers*, SPIE, Long Beach, CA **2021**.
- [50] K. Barri, P. Jiao, Q. Zhang, J. Chen, Z. L. Wang, A. H. Alavi, *Nano Energy* **2021**, *86*, 106074.
- [51] S. Wang, L. Lin, Z. L. Wang, *Nano Lett.* **2012**, *12*, 6339.
- [52] G. Zhu, C. Pan, W. Guo, C.-Y. Chen, Y. Zhou, R. Yu, Z. L. Wang, *Nano Lett.* **2012**, *12*, 4960.
- [53] S. Niu, Z. L. Wang, *Nano Energy* **2014**, *14*, 161.
- [54] H. J. Sim, C. Choi, S. H. Kim, K. M. Kim, C. J. Lee, Y. T. Kim, X. Lepró, R. H. Baughman, S. J. Kim, *Sci. Rep.* **2016**, *6*, 35153.
- [55] R. Sovják, P. Havlásek, J. Vítek, *Constr. Build. Mater.* **2018**, *188*, 781.
- [56] Y. Zi, J. Wang, S. Wang, S. Li, Z. Wen, H. Guo, Z. L. Wang, *Nat. Commun.* **2016**, *6*, 1.
- [57] S. Niu, S. Wang, L. Lin, Y. Liu, Y. Zhou, Y. Hu, Z. L. Wang, *Energy Environ. Sci.* **2013**, *6*, 3576.
- [58] L. Y. Wang, W. A. Daoud, *Adv. Energy Mater.* **2019**, *9*, 1803183.
- [59] H. Qin, G. Cheng, Y. Zi, G. Gu, B. Zhang, W. Shang, F. Yang, J. Yang, Z. Du, Z. L. Wang, *Adv. Funct. Mater.* **2018**, *8*, 1805216.
- [60] H. Qin, G. Gu, W. Shang, H. Luo, W. Zhang, P. Cui, B. Zhang, J. Guo, G. Cheng, Z. Du, *Nano Energy* **2020**, *68*, 104372.
- [61] W. Shang, G. Gu, W. Zhang, H. Luo, T. Wang, B. Zhang, J. Guo, P. Cui, F. Yang, G. Cheng, Z. Du, *Nano Energy* **2021**, *82*, 105725.
- [62] J. Park, S. Choi, H. M. Jung, *Appl. Sci.* **2020**, *10*, 6754.
- [63] A. H. Alavi, H. Hasni, N. Lajnef, K. Chatti, F. Faridazar, *Autom. Constr.* **2016**, *62*, 24.
- [64] A. H. Alavi, H. Hasni, P. Jiao, W. Borchani, N. Lajnef, *J. Constr. Steel Res.* **2017**, *128*, 19.
- [65] K. Barri, Q. Zhang, D. Mehta, S. Chakrabarty, R. E. Debski, A. H. Alavi, in *Proc. of the American Professional Society of Photographic Instrumentation Engineers*, SPIE, Long Beach, CA **2021**.
- [66] D. Mehta, K. Aono, S. Chakrabarty, *Nat. Commun.* **2020**, *11*, 5446.
- [67] M. H. Malakooti, H. A. Sodano, *Smart Mater. Struct.* **2015**, *24*, 055005.
- [68] G. Zhao, Y. Zhang, N. Shi, Z. Liu, X. Zhang, M. Wu, C. Pan, H. Liu, L. Li, Z. L. Wang, *Nano Energy* **2019**, *59*, 302.
- [69] W. Zhang, G. Gu, H. Qin, S. Li, W. Shang, T. Wang, B. Zhang, P. Gui, J. Guo, F. Yang, G. Cheng, Z. Du, *Nano Energy* **2020**, *77*, 105108.
- [70] W. Zhang, G. Gu, W. Shang, H. Luo, T. Wang, B. Zhang, P. Cui, J. Guo, F. Yang, G. Cheng, Z. Du, *Nano Energy* **2021**, *86*, 106056.
- [71] J. R. Barber, *Elasticity*, Spinger, New York **2010**.